Journal of Materials Chemistry C

ROYAL SOCIETY OF CHEMISTRY

PAPER

View Article Online
View Journal | View Issue

Cite this: J. Mater. Chem. C, 2022, 10, 3819

Synthesis of magnetic nanoparticles by laser ablation of strontium ferrite under water and their characterization by optically detected magnetophoresis supported by BEM calculations†

Valentina Piotto, ‡[a] Lucio Litti, ‡[a] Alexander Omelyanchik,§[b] Alessandro Martucci,[c] Piero Riello,[d] Davide Peddis[b] and Moreno Meneghetti *[a]

Measurement of the properties of magnetic nanoparticles is mandatory for their application and usually this is accomplished using magnetometers, like SQUIDs or VSMs. However, these techniques require amounts of materials that are not always available and do not allow exploration of new syntheses with low production. The tiny quantity of nanoparticles obtained by laser ablation of strontium ferrite necessitated the characterization of their magnetic properties using an alternative technique, optically detected magnetophoresis, which exploits the motion of nanoparticles in a fluid under a magnetic field gradient. Time dependent optical extinction of a colloidal solution of magnetic nanoparticles can be used for recording the collective motion of the nanoparticles in a fluid. The optical extinction of nanoparticles, with absorption and scattering contributions, depends on the particle material and on their morphologies. We report a new implementation of a magnetophoretic model with the extinction properties of nanoparticles calculated using the Boundary Element Method. The model is applied to estimate the magnetic properties of a challenging sample of mixed ferrite nanoparticles. The results show that, especially for polydisperse samples, the explicit consideration of the size dependent extinction properties of the nanoparticles is needed to characterize magnetic nanoparticles by optically detected magnetophoresis. The motion of magnetic nanoparticles in a fluid, exploited in many applications, is provided with an appropriate description using the present approach.

Received 7th October 2021,
Accepted 27th January 2022

DOI: 10.1039/d1tc04796e

rsc.li/materials-c

Introduction

Magnetic nanoparticles (MagNPs) attract increasing interest in several technological applications like high density data storage,[1] ferrofluids,[2,3] nanolubricants,[4] and waste water treatment,[5] and in biomedical applications like remote cell manipulation[6–8] or drug delivery,[9,10] multimodal SERS/MRI contrast agents[11–13] and magnetic hyperthermia.[14,15] Understanding the effect of an applied magnetic field on MagNPs provides fundamental knowledge for improving their applications. The SQUID (Superconducting QUantum Interference Device) is a magnetometer usually considered for the measurement of the magnetic properties of materials. However, this technique usually requires an amount of sample that is not always available, in particular when new syntheses of MagNPs are explored. Another magnetometer, a VSM (vibrating-sample magnetometer), frequently used for characterizing magnetic materials, suffers from the same problem.

The magnetic behaviour of nanoparticles can be also studied through the direct or indirect observation of their motion in a fluid under an external magnetic field gradient, a process called magnetophoresis. The trajectories of single magnetic particles in a liquid can be directly measured using an optical microscope when particles have dimensions of at least several micrometers,[16–18] whereas the motion of an ensemble of nanoparticles can be indirectly recorded by recording the variation

[a] Department of Chemical Sciences, University of Padova, via Marzolo 1, 35131 Padova, Italy. E-mail: moreno.meneghetti@unipd.it
[b] Department of Chemistry and Industrial Chemistry, University of Genova, via Dodecaneso 31, 16146 Genova, Italy
[c] Department of Industrial Engineering, University of Padova, via Marzolo, 35131 Padova, Italy
[d] Department of Molecular Sciences and Nanosystems, Università Ca' Foscari Venezia, 30170 Mestre, Venezia, Italy

† Electronic supplementary information (ESI) available: Supplementary discussion about Brownian motion of particles under a magnetic field, BEM simulations, supplementary magnetic characterization and EDX analysis, scheme of the magnetophoretic experiment. See DOI: 10.1039/d1tc04796e

‡ These authors equally contributed to this work.

§ Present address: Immanuel Kant Baltic Fed Univ, Inst Phys Math & Informat Technol, Kaliningrad 236001, Russia.

of the optical extinction of a solution under the influence of a magnetic field gradient.[19,20] In particular, the last technique, optically detected (OptD) magnetophoresis, is appropriate when a small amount of nanoparticles are available. Based on this approach, Helseth and Skodvin[19] explored samples with different degrees of dimensional polydispersity using micron-sized iron oxide nanoparticles, whereas Andreu *et al.* considered the magnetophoretic behaviour of core (γ-Fe_2O_3) and core–shell (γ-Fe_2O_3@SiO_2) nanoparticles in studying aggregation processes of nearly monodisperse nanoparticles, which can be another source of polydispersity.[21]

Nanoparticles of different dimensions have different wavelength dependent extinction properties, namely absorption plus scattering properties, and knowledge about them is important for fitting the OptD magnetophoretic data. A model that includes these properties, exploiting the OptD magnetophoretic experimental data, was not previously considered.

In the present work we show the importance of including the size dependent extinction properties of magnetic nanoparticles in a model for fitting the OptD magnetophoretic experimental data. Boundary Element Method calculations are used to obtain the extinction properties of nanoparticles of different sizes.

After reporting how the magnetophoretic model can be exploited, it is applied to the characterization of polydisperse magnetic nanoparticles obtained by ablation of a strontium ferrite target under water.

Experimental

Synthesis of magnetic nanoparticles

Laser ablated magnetic nanoparticles were obtained with 9 ns pulses of a doubled Nd:YAG laser (Quantel, model: Q-smart 450) at 532 nm ablating a strontium ferrite target, provided by Supermagnete (Fe–S–05–05, Y35), covered with double distilled water. Ablation was conducted with a 2 J cm^{-2} fluence at 20 Hz. The ablation used 5 mL of water over the target and was continued for 12 minutes. The colloidal sample was cleaned by acid treatment to dissolve the hydroxides that are observed around the nanoparticles by TEM images. This was obtained by dispersing the nanoparticles in dilute HCl at pH 1.3. After a brief sonication for one minute, nanoparticles were magnetically attracted for 30 minutes. This procedure allowed nonmagnetic nanoparticles and very small nanoparticles that did not reach the magnet within 30 minutes to be discarded. After this, the attracted nanoparticles were redispersed in double distilled water and a short (10 minutes) magnetic attraction was used for discarding very big or aggregated nanoparticles, recovering the nanoparticles that were present in the solution.

Raman spectra (see below) were used to verify that the composition of the nanoparticles from different syntheses was constant.

Characterization of nanoparticles

The dimensional distribution of nanoparticles was evaluated using an FEI TECNAI G2 transmission electron microscope operating at 100 kV, while the hydrodynamic size was measured using a Malvern Instrument Zetasizer Nano. UV-vis-NIR extinction spectra were acquired using a Cary 5000 spectrophotometer (Agilent Technologies) with a 2 mm optical path quartz cuvette. Raman measurements were recorded using a Renishaw inVia micro-Raman spectrometer with a 514 nm exciting laser beam focused on dried samples with a 20x objective. Atomic composition analysis was performed using a Zeiss Sigma SEM microscope equipped with an EDX from Oxford Instruments (x-act PentaFET Precision). The sample was deposited by drop casting on a Ge substrate. The instrument was operated at 20 kV and the spectrum was recorded up to an energy of 10 keV. The software used for the analysis also considered ZAF correction. For the quantitative analyses of Fe and Sr, the peak of Fe ($K_{\alpha1}$, $K_{\alpha2}$) at 6.40 keV and that of Sr ($L_{\alpha1}$, $L_{\alpha2}$, L_{β}) at 1.83 keV were used, consistent with the instrument calibration performed at the same accelerating voltage of 20 kV.

Ellipsometry measurements were conducted using a V-VASE (J. A. Wollman Co.) ellipsometer.

Experimental set-up for magnetophoresis

OptD magnetophoresis curves were recorded using a home-made magnetophoretic cell, made of Teflon and two quartz windows. The cell has a volume of 0.3 cm^3, an optical path of 1 cm and a section area of 0.3×1.0 cm^2. Fig. S9 (ESI†) presents a scheme of the magnetophoretic cell and of the experiment. The magnet (NdFeB, S-10-20-N, N45, Supermagnete) was incorporated in the Teflon side of the cell. The magnetic gradient was, therefore, perpendicular to the optical path with the flat surface of the magnet in contact with the liquid. The magnetic field of the magnet was measured using a ''400 series'' Hall effect probe coupled with a Lake Shore model 475 DSP gaussmeter. 300 μL of colloidal solution completely covered the magnet face in contact with the solution. As soon as the sample was introduced in the magnetophoretic cell, the extinction of the solution was recorded at a fixed wavelength as a function of time. The magnetophoretic model for fitting the experimental data was implemented using Matlab R2017b.

BEM simulations

The Boundary Element Method (BEM) was used to simulate the extinction properties of the nanoparticles with the given shapes and dimensions.[22] A Matlab R2017b code based on libraries written by Hohenester *et al.*[23] was used for the BEM calculations.

Results and discussion

In a magnetophoretic experiment the motion of magnetic nanoparticles (MagNP) in a liquid under the influence of a magnetic field gradient is recorded. Diluted colloidal solutions

avoid magnetic dipole–dipole interactions among nanoparticles and their motion is driven by the magnetic (F_m) and drag (F_{drag}) forces.

The magnetic force F_m on a MagNP immersed in a fluid is[24–26]

$$F_m = V_{MNP}\, M(H)\nabla B \quad (1)$$

where V_{MNP} is the nanoparticle magnetic volume and ∇B is the gradient of the magnetic field. $M(H)$ is the magnetization of the nanoparticle, which is dependent on the applied magnetic field.

The drag force F_{drag} is determined by the liquid and counteracts the magnetic force. Its modulus is proportional to the velocity of the nanoparticles according to the Stokes equation:

$$F_{drag} = 3\pi D_h \eta v(z) \quad (2)$$

where D_h is the hydrodynamic diameter of the nanoparticle, η is the dynamic viscosity of the liquid and $v(z)$ is the velocity of the MagNP in the z direction, namely the magnetic axis.

The force on a nanoparticle very quickly becomes null when F_{drag} increases to the value of F_m. The drift velocity becomes constant when the two forces compensate to the value:

$$v(z) = \frac{V_{MNP} M(H) \nabla B(z)}{3\pi D_h \eta} \quad (3)$$

The NdFeB magnet present in the magnetophoretic cell used for the experiments (see Materials and Methods) creates a magnetic field of 0.55 T at the surface of the magnet and of 0.24 T at a distance of 3 mm, whereas the gradient of the field, along the z-direction, perpendicular to the magnet surface, slightly increases towards the magnet with an average value around 100 T m^{-1} (see the ESI,† Section 3). Since the gradient is small, the model discretizes the z-axis in steps, considering it constant in each step. The magnetophoretic curve, namely the time dependent optical extinction of the colloidal solution, is experimentally obtained using a UV-vis-NIR spectrophotometer, recording the extinction at a given wavelength as a function of time. The extinction of the colloidal solution is then fitted by summing the contributions of all the nanoparticles initially distributed uniformly within the whole volume of the sample.

The motion of the nanoparticles, especially at room temperature and with smaller sizes, is also influenced by the Brownian motion. A detailed discussion of its influence on the magnetophoretic curve, considering the experimental set-up of the present work, can be found in Section 1 of the ESI.† Brownian diffusion influences in particular small particles and it is shown that, because of the compensation effect determined by the distribution of nanoparticles starting their motion from different distances from the magnet surface, it has a minor influence on the magnetophoretic curve.

Each nanoparticle shows an extinction spectrum, which depends on the material of the nanoparticle, but also on its size, and can be obtained by the sum of the scattering and absorption contributions. Considering the UV-vis-NIR spectral regions, particles with increasing dimensions from tens to hundreds of nanometers can show a significant wavelength dependent extinction.

The calculation of the optical extinction of the nanoparticles can be made using the Boundary Element Method.[22,23] The calculations can be performed using the dielectric function or, equivalently, the complex refractive index of the bulk material.

An example of the calculated extinction cross section of magnetite nanoparticles dispersed in water and with increasing diameters, from 10 to 500 nm, is shown in Fig. 1a and b. The corresponding scattering and absorption contributions are shown in Fig. S4 of the ESI.† In particular, one can see that, with increasing dimension of a nanoparticle, a shift in the extinction spectrum toward longer wavelengths can be observed.[27]

These results underline the importance of considering the extinction contributions of nanoparticles of different sizes.

Demonstration of the influence of the extinction of magnetite nanoparticles is shown in Fig. 2a with size distributions presented in Fig. 2b. In these calculations the hydrodynamic diameter is considered equal to the physical one, the magnetization is set at 80 A m^2 kg^{-1}[28] and the nanoparticles, randomly distributed in the whole solution volume, move under the influence of the gradient of the magnetic field used in all

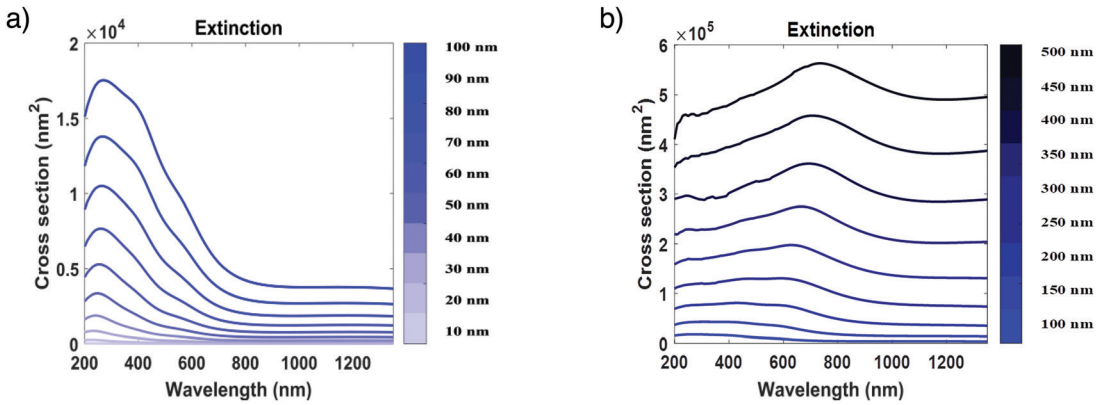

Fig. 1 BEM extinction spectra calculated for magnetite nanoparticles with diameters from 10 to 100 nm (a) and from 100 to 500 nm (b).

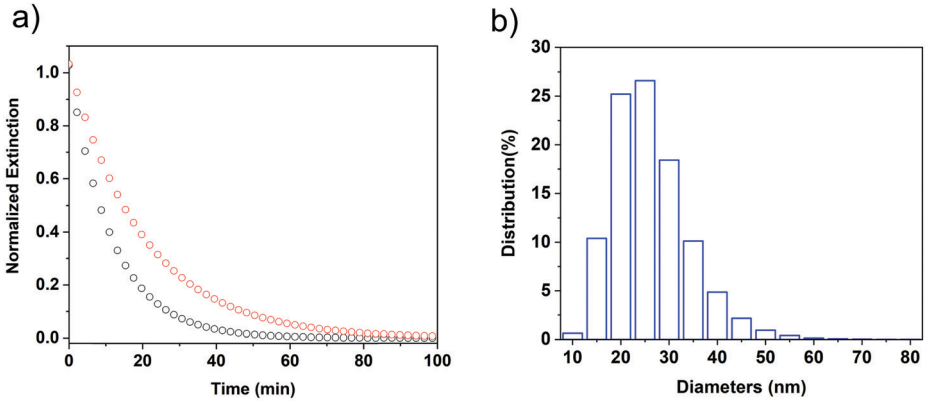

Fig. 2 (a) Magnetophoretic curve of an ideal sample of magnetite nanoparticles with the size distribution shown in (b). The red line shows the simulation without considering the extinction contribution of nanoparticles with different diameters, whereas the black line is obtained by including the extinction of the nanoparticles shown in Fig. 1.

the magnetophoretic experiments, which is shown in Fig. S5b (ESI†). The magnetophoretic curve is calculated by summing, for all nanoparticle sizes, the extinction at 440 nm, which accounts for both large and small nanoparticles. The difference between the two curves in Fig. 2a underlines the importance of considering the correct extinction of the nanoparticles. One can also observe that the calculated total time to attract all the nanoparticles without including the size dependent extinction is almost doubled.

An application of the above model is reported below for magnetic nanoparticles obtained by laser ablation under water of a strontium ferrite sample (see Experimental). This sample represents a double challenge, first because of the low yield of the laser ablation synthesis, making it difficult to measure the magnetic properties of the nanoparticles using usual magnetometers, and second because its intrinsic properties, like polydispersity and material composition, reflect the complexity of the sample. After the ablation synthesis, the nanoparticles were purified from hydroxides by acid treatment and selected with double magnetic attraction (see Experimental).

Since laser ablation under water usually favours the presence of oxides, we used Raman spectroscopy for the qualitative evaluation of the composition of the nanoparticles, whereas an EDX analysis was used for the evaluation of the atomic ratio of Fe/Sr. XRD could not be used for the small quantity of the synthesized sample.

The Raman spectrum of strontium ferrite is characterized by a low intensity band at about 700 cm^{-1} where also a band of a magnetic phase of iron oxide, namely magnetite, is present.[29,30] However, magnetite transforms into hematite under the action of the laser used for recording the Raman spectrum, if the power is high, whereas this is not observed for strontium ferrite. Fig. S6 (see the ESI†) shows the Raman spectra of the ablated sample, pure magnetite and pure strontium ferrite irradiated with a 514 nm laser beam, using a 20× objective, at low (0.5 mW, black lines) and high levels of irradiation (25 mW for 1 minute, red lines). For magnetite (Fig. S6c, ESI†), a band at about 700 cm^{-1} is no longer present after irradiation at a high power because the magnetite transformed into hematite, which is characterized by two intense bands at 210 and 270 cm^{-1}, whereas the pure strontium ferrite spectrum is stable also under high power irradiation (Fig. S6b, ESI†), although with some frequency changes. From the spectrum of the ablated sample (Fig. S6a, ESI†), one can recognize, after high-power irradiation, the bands of both strontium ferrite and hematite. The Raman spectra show, therefore, that the ablated sample contains both magnetite and strontium ferrite.

EDX measurements (Fig. S8, ESI†) confirmed the presence of Sr and the atomic ratio of Fe/Sr was found to be 27 ± 1. Considering that strontium ferrite and magnetite are present, the Fe/Sr ratio is 1 : 5 between these two magnetic materials. It is known that the atomic ratio obtained by the EDX measurement can be affected by geometrical factors like the structure of nanoparticles. For this reason we used (see below) the ratio to calculate the extinction spectrum of the colloidal solution and found a good agreement with the experimental spectrum, showing that the EDX result can be considered reliable. EDX measurements did not demonstrate the variation of the ratio of Fe/Sr in different parts of the sample also for almost isolated particles (see Fig. S8, ESI†). This strongly suggested that the nanoparticles have mixed phases with an important transformation of the initial ablated strontium ferrite material in the water environment.

The distribution of the diameters of the cleaned nanoparticles, obtained through TEM images (see Fig. 3b), is shown in Fig. 3c. A lognormal distribution fitting shows that the nanoparticles are characterized by a mean value of 80 nm and a variance of 69 nm. Given the large dispersion, and according to the manufacturer guidelines, the DLS measurements of the hydrodynamic diameter of the nanoparticles were not reliable. Therefore, the diameters of the nanoparticles were set to the dimensions observed by TEM (see Fig. 3c), which can be a sufficient approximation in particular for large nanoparticles with a clean surface like the ablated ones after the acid treatment. The TEM images of these nanoparticles show, in fact, that the hydroxides are no longer present on the surface of the nanoparticles after the acid treatment (see Fig. 3b), and cannot influence the hydrodynamic diameters of the nanoparticles.

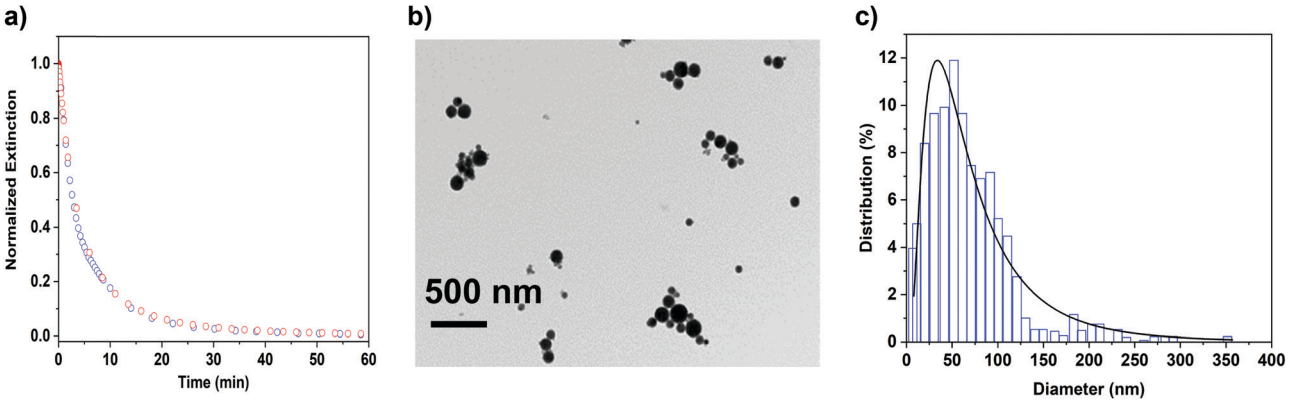

Fig. 3 (a) The experimental magnetophoretic curve (red circles) with the fitting (blue circles) obtained with a magnetization of 11 Am^2 kg^{-1}. (b) TEM images of the nanoparticles and (c) dimensional distribution of 400 nanoparticles synthesized by laser ablation of strontium ferrite.

The experimental magnetophoretic curve of a colloidal solution at a concentration of 80 mg L^{-1}, which allows dipole–dipole interactions among nanoparticles to be avoided (see the ESI,† Section 4), is shown in Fig. 3a (red circles). The curve was obtained by recording the extinction of the colloidal solution at 440 nm, since at this wavelength both small and large nanoparticles contribute to the extinction (see below).

As shown above, for the fitting of the magnetophoretic curve, the extinction properties of the nanoparticles as a function of their dimensions need to be known. The extinction properties of the magnetite nanoparticles are shown in Fig. 1. For strontium ferrite the real and imaginary parts of the refractive index, needed for the calculation of the optical extinction, were not available and we obtained them using an ellipsometric measurement of a polished surface of one of the magnets used for the laser ablation. Fig. 4a presents the obtained real and imaginary parts of the refractive index of strontium ferrite.

We performed BEM calculations for nanoparticles with different dimensions and the composition determined for the

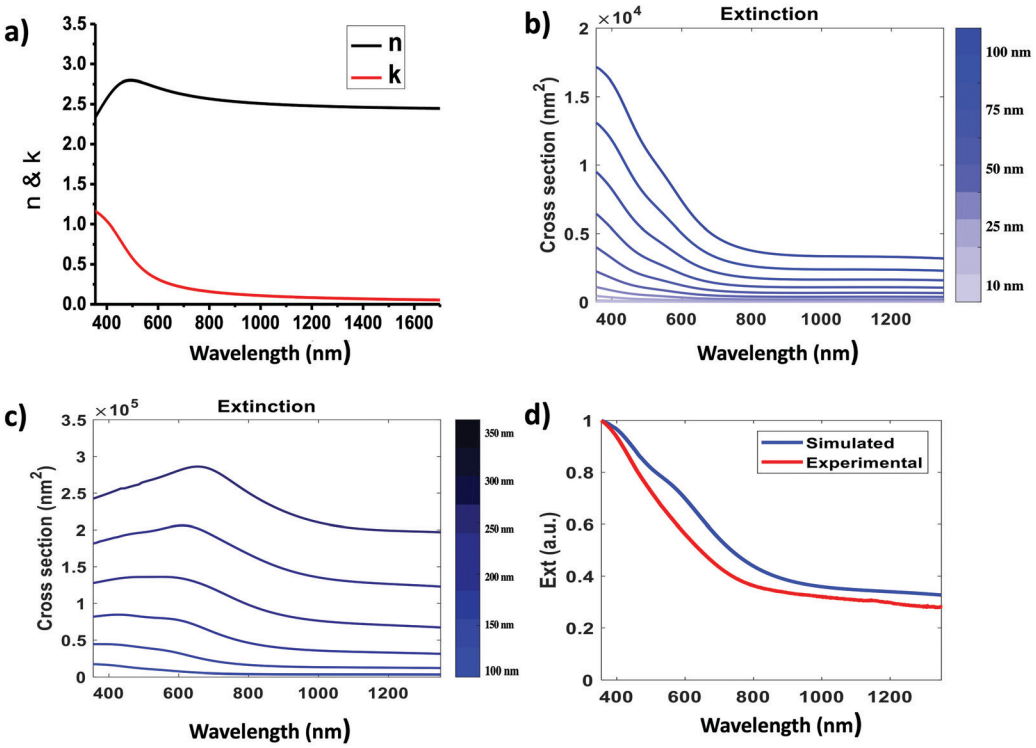

Fig. 4 (a) Real (*n*) and imaginary (k) parts of the refractive index of strontium ferrite. (b and c) BEM calculations of the extinction of nanoparticles with a 1 : 4.9 strontium ferrite and magnetite composition. Calculated spectra are reported for nanoparticles with sizes between 10 and 100 nm (b) and between 100 and 350 nm (c). (d) Experimental (red line) and calculated (blue line) extinction spectra of the nanoparticles with the dimensional distribution presented in Fig. 4a.

presence of magnetite and strontium ferrite suggested by the EDX measurement. Fig. 4b and c show the calculated extinction spectra of the nanoparticles of different dimensions and the fitting of the experimental extinction spectra of the colloidal solution of the ablated nanoparticles based on the contribution of the nanoparticles of different dimensions (see Fig. 4d). The fitting can be considered satisfactory given the complex composition of the nanoparticles.

Given the calculated extinction at 440 nm of the nanoparticles of different dimensions, showing a contribution of both small and large nanoparticles, and given their distribution, we obtained the fitting (Fig. 3a, blue circles) of the magnetophoretic curve using the magnetization of the nanoparticles as a fitting parameter.

The fitting well reproduces the experimental data using a magnetization of 11 A m^2 kg^{-1} (the density of magnetite and strontium ferrite is 5.18 g cm^{-3}). Compared to pure magnetite, this value is about seven times lower. Even considering the presence of strontium ferrite, with a lower magnetization than magnetite, the estimated magnetization is low. This can be understood considering that the mixed phases of strontium ferrite and magnetite are highly disordered with no well-defined magnetic domains.

The characterization of the magnetic properties of the nanoparticles obtained by the ablation of a $SrFe_{12}O_{19}$ magnet shows that they can be used for magnetophoretic experiments, but not for highly-demanding applications.

Conclusions

Magnetic nanoparticles are used in several fields and the characterization of their magnetic properties is an important step. Standard techniques require an amount of sample that is not always available, in particular when new syntheses are explored. The optically detected magnetophoresis, namely the time dependent optical extinction of a colloidal solution of nanoparticles under the influence of a magnetic field gradient, can be a valid alternative for the characterization of the magnetic properties of tiny amounts of nanoparticles. We have shown the importance of considering the extinction of nanoparticles of different dimensions through BEM calculations. The model was applied to a complex sample of magnetic nanoparticles obtained by the laser ablation of a strontium ferrite target. The magnetization of the ablated nanoparticles was found to be weak.

The results show that the magnetophoretic measurement supported by BEM calculations can be considered a valid approach for characterizing the magnetic properties of small amounts of magnetic nanoparticles.

Author contributions

V. P. synthesized and characterized the nanoparticles and recorded the experimental magnetophoretic curves. V. P. and L. L. implemented the magnetophoretic model and BEM simulations. A. M. recorded the ellipsometry data. A. O. and D. P. performed the magnetic measurements. P. R. recorded the XRD data. M. M. defined and critically followed the development of the project and prepared the manuscript with V. P. and L. L. All the authors contributed to data discussion.

Conflicts of interest

There are not conflicts to declare.

Acknowledgements

M. M. would like to acknowledge funding from the University of Padova, project P-DiSC#06BIRD2020-UNIPD. Special acknowledgements to Andrea Basagni for the EDX measurements, to the Cloud Veneto computational facility for providing the resources for the BEM simulations and to Lorenzo Dainese for the customization of the magnetophoretic cell.

Notes and references

1 J. H. Park, C. Park, T. Jeong, M. T. Moneck, N. T. Nufer and J. G. Zhu, *J. Appl. Phys.*, 2008, **103**, 07A917.
2 C. Rigoni, D. Ferraro, M. Carlassara, D. Filippi, S. Varagnolo, M. Pierno, D. Talbot, A. Abou-Hassan and G. Mistura, *Langmuir*, 2018, **34**, 8917–8922.
3 B. Y. Hui, N. N. M. Zain, S. Mohamad, P. Varanusupakul, H. Osman and M. Raoov, *Food Chem.*, 2020, **314**, 126214.
4 V. Zin, F. Agresti, S. Barison, L. Litti, L. Fedele, M. Meneghetti and M. Fabrizio, *Tribol. Int.*, 2018, **127**, 341–350.
5 A. Abd Aziz, K. S. Yong, S. Ibrahim and S. Pichiah, *J. Hazard. Mater.*, 2012, **199**, 143–150.
6 F. Bertorelle, M. Pinto, R. Zappon, R. Pilot, L. Litti, S. Fiameni, G. Conti, M. Gobbo, G. Toffoli, M. Colombatti, G. Fracasso and M. Meneghetti, *Nanoscale*, 2018, **10**, 976–984.
7 D. Calzavara, D. Ferraro, L. Litti, G. Cappozzo, G. Mistura, M. Meneghetti and M. Pierno, *Adv. Condens. Matter Phys.*, 2018, **2018**, 2849175.
8 T. Xue, S. Q. Wang, G. Y. Ou, Y. Li, H. M. Ruan, Z. H. Li, Y. Y. Ma, R. F. Zou, J. Y. Qiu, Z. Y. Shen and A. G. Wu, *Anal. Methods*, 2019, **11**, 2918–2928.
9 J. Park, M. A. Castanares, D. S. Collins and Y. Yeo, *Mol. Pharmaceutics*, 2019, **16**, 1864–1873.
10 N. Depalo, R. M. Iacobazzi, G. Valente, I. Arduino, S. Villa, F. Canepa, V. Laquintana, E. Fanizza, M. Striccoli, A. Cutrignelli, A. Lopedota, L. Porcelli, A. Azzariti, M. Franco, M. L. Curri and N. Denora, *Nano Res.*, 2017, **10**, 2431–2448.
11 C. Scialabba, R. Puleio, D. Peddis, G. Varvaro, P. Calandra, G. Cassata, L. Cicero, M. Licciardi and G. Giammona, *Nano Res.*, 2017, **10**, 3212–3227.

12 J. Reguera, D. J. de Aberasturi, M. Henriksen-Lacey, J. Langer, A. Espinosa, B. Szczupak, C. Wilhelm and L. M. Liz-Marzan, *Nanoscale*, 2017, **9**, 9467–9480.
13 Y. Han, S. L. Lei, J. H. Lu, Y. He, Z. W. Chen, L. Ren and X. Zhou, *Mater. Sci. Eng., C*, 2016, **64**, 199–207.
14 B. T. Mai, P. B. Balakrishnan, M. J. Barthel, F. Piccardi, D. Niculaes, F. Marinaro, S. Fernandes, A. Curcio, H. Kakwere, G. Autret, R. Cingolani, F. Gazeau and T. Pellegrino, *ACS Appl. Mater. Interfaces*, 2019, **11**, 5727–5739.
15 X. Wang, F. Pan, Z. Xiang, W. W. Jia and W. Lu, *Mater. Lett.*, 2020, **262**, 127187.
16 N. Kohama, C. Suwabe, H. Ishii, K. Hayashi and D. Nagao, *Colloids Surf., A*, 2019, **568**, 141–146.
17 J. Nguyen, D. V. Conca, J. Stein, L. Bovo, C. A. Howard and I. L. Garcia, *Proc. Natl. Acad. Sci. U. S. A.*, 2019, **116**, 2425–2434.
18 D. T. Grob, N. Wise, O. Oduwole and S. Sheard, *J. Magn. Magn. Mater.*, 2018, **452**, 134–140.
19 L. E. Helseth and T. Skodvin, *Meas. Sci. Technol.*, 2009, **20**, 095202.
20 R. Fabbro, J. Fournier, P. Ballard, D. Devaux and J. Virmont, *J. Appl. Phys.*, 1990, **68**, 775–784.
21 J. S. Andreu, J. Camacho, J. Faraudo, M. Benelmekki, C. Rebollo and L. M. Martinez, *Phys. Rev. E: Stat., Nonlinear, Soft Matter Phys.*, 2011, **84**, 021402.
22 L. Litti and M. Meneghetti, *Phys. Chem. Chem. Phys.*, 2019, **21**, 15515–15522.
23 U. Hohenester and A. Trugler, *Comput. Phys. Commun.*, 2012, **183**, 370–381.
24 M. Iranmanesh and J. Hulliger, *Chem. Soc. Rev.*, 2017, **46**, 5925–5934.
25 J. F. Schenck, *J. Magn. Reson. Imaging*, 2000, **12**, 2–19.
26 J. F. Schenck, *Prog. Biophys. Mol. Biol.*, 2005, **87**, 185–204.
27 B. Sinha, T. Goswami, S. Paul and A. Misra, *RSC Adv.*, 2014, **4**, 5092–5104.
28 S. J. Kemp, R. M. Ferguson, A. P. Khandhar and K. M. Krishnan, *RSC Adv.*, 2016, **6**, 77452–77464.
29 L. Balcells, C. Martinez-Boubeta, J. Cisneros-Fernandez, K. Simeonidis, B. Bozzo, J. Oro-Sole, N. Bagues, J. Arbiol, N. Mestres and B. Martinez, *ACS Appl. Mater. Interfaces*, 2016, **8**, 28599–28606.
30 C. Y. Zhao, M. Y. Shen, Z. X. Li, R. Sun, A. L. Xia and X. G. Liu, *J. Alloys Compd.*, 2016, **689**, 1037–1043.